Optimisation and Design Performance of a Small-Scale DC Vernier Reluctance Machine for Direct-Drive Wind Generator Drives

Udochukwu B. Akuru
Dept. of Electrical Engineering
Tshwane University of Technology
Pretoria, South Africa
AkuruUB@tut.ac.za

Maarten J. Kamper and Mkhululi Mabhula
Dept. of Electrical and Electronic Engineering
Stellenbosch University
Stellenbosch, South Africa
kamper@sun.ac.za, mabhulamkhululi@gmail.com

***Abstract*—The study begins with a proposal to design a small-scale DC Vernier reluctance machine (DC-VRM) for direct-drive wind generator drives. The motivation centres on the increasing need for renewable energy technologies, as well as the quest for non-PM and gearless wind generator drives upon which the DC-VRM is uniquely compatible. A global optimisation is first undertaken based on solutions from 2D finite element modelling (FEM) to produce optimal benchmark designs (OBDs). The OBDs are further evaluated for independent performance improvement of the torque ripple using the simple rotor tooth-pairing technique. The findings show that the torque ripple can be drastically reduced when absolved from the integrated optimisation process. On the average, at 0.8 tooth-paring ratio, the torque ripple reduces by at least by 50 %, with observation of special quid pro quo effects in torque ripple and average torque generation of this machine. Already, 3D FEM simulations have been issued to draw out the end-effect discrepancies, while laboratory validation is still pending.**

Keywords—DC Vernier reluctance machine, finite element modelling, optimisation, torque ripple, wind generator drives

I. Introduction

Stator-mounted double-salient wound-field machines are lately becoming interesting machine variants due to avoidance of expensive PMs, less copper volume mainly as a result of concentrated winding layouts, robust rotor topologies, as well as easy thermal management. Among these machine variants, the DC-excited Vernier reluctance machine (DC-VRM) [1] stands out due to extended operational limits and improved machine reliability in terms of its propensity for brushless and adjustable DC field exciters. However, a major challenge for these machines is an overwhelmed stator comprising both DC field- and AC phase-windings which tend towards increasing and complicating the magnetic activity in the stator core, resulting into short-term saturation [2].

Besides, due to its double salient structure, torque ripple, is a cause for worry. This is caused by slotting effects of the stator and rotor MMF harmonics on the airgap permeance [2], as well as non-symmetric flux linkage and back EMF waveform exhibition at rated operating points [3], leading to mechanical vibrations and acoustics. Notwithstanding, due to the design composition (brushless and no slip-rings), as well as performance implication (high torque density) of these machine topologies [4], they cannot be overlooked for wind power generation.

Meanwhile, renewable energy technology, which includes wind power generation, is presently attracting widespread interest because of its crucial role in addressing climate change and increasing electricity access, among others [5]. To this end, this study is based on the optimisation and design of a 15 kW three-phase DC-VRM direct-drive wind generator drive, patterned after a 7.2 m diameter wind turbine [6]. Based on available turbine power curves, the turbine operating speed is pegged at 200 r/min, with a rated wind speed of ~10 m/s. In recent times, the popularity of direct-drive wind generator drive technologies is growing, given that they do not integrate gearboxes in their drivetrains and as such, guarantee a simplified drivetrain architecture, while reducing maintenance and operational costs [7].

Regarding the emergence of brushless stator-mounted wound-field machines, it is unknown that the DC-VRM has been investigated in the past as anticipated in this study, unlike counterparts such as the so-called wound-field flux switching machine (WF-FSM) and DC-excited flux reversal machine (DC-FRM) [8]-[10], to mention a few. In [9], a 10 kW WF-FSM wind generator drive is prototyped and tested to exhibit the ease of the manufacturing process. In [10], a 22 kW four-phase DC-FRM is artfully designed to mimic the characteristics of its PM-FRM counterpart and offer controllable DC field versus output power range despite varying wind profile. Unlike these few examples with DC field-excitation, it is more commonly seen that PM-excited stator-mounted machines are being employed in the small-scale wind power range and for multi-phase designs [8], [10]-[12].

For the proposed DC-VRM wind generator, the potential disruptions and cost per capita posed by price fluctuations of expensive rare-earth PMs used for conventional wind generator designs are allayed, being 'completely' rare-earth free [13]. DC-VRM exercises a much simpler winding layout compared to WF-FSM or DC-FRM since the DC field- and AC phase-windings can be concentrated and wound on the same stator pole arm. Besides, with a penchant for high number of poles (rotor teeth), the three-phase DC-VRM design not only promotes design and control simplicity, but is well-suited for the proposed direct-drive wind turbine systems [14]. It is on this basis that the novelty of this study has been contemplated. It should be said that the study is mainly concerned with the electromagnetic design and optimisation strategy of the proposed wind generator drive. Hence, inferences made towards the drive performance, which is highlighted due to the overall wind turbine architecture, should only be assessed in terms of kVA/costs of the power converters.

The study is based on 2D finite element modelling (FEM), upon which the wind generator concept is developed and analysed. Multi-objective design optimisation is then

U. B. Akuru is also affiliated with the Department of Electrical and Electronic Engineering, Stellenbosch University, South Africa, and the Department of Electrical Engineering, University of Nigeria, Nsukka.

undertaken, following which a simple parametric analysis is conducted to address prominent torque ripple effects in three selected optimum benchmark designs (OBDs). The OBDs are then compared for performance with a standard 15 kW non-overlap-winding (NO) PMSG [15]. At the end of the study, an initial account on benchmark concept validation is given based on 3D FEM simulations, while practical development and testing of a laboratory prototype is emphasized but yet to be completed due to outbreak of the COVID-19 pandemic.

II. Concept Theory and Design Specifications

As earlier mentioned, DC-VRMs are double-salient machines, housing both DC and AC windings on the stator. The AC windings can either be in concentrated or distributed layouts, depending on whether the pole ratio is less or greater than 3, respectively [14]. An overwhelming analysis of the theory of operation of DC-VRMs using the winding function theory and harmonic analysis has been carried out in [14] of which it sums to the flux modulation being a result of the rotating permeance acting on a stationary DC MMF. By further interactions of the modulated DC field harmonics with that of the AC MMF harmonics, torque can be produced only if both harmonics exhibit the same:

- spatial orders, and
- rotational direction and frequencies.

A 3-phase 12-stator/10-rotor slots radial-flux concentrated winding design topology is selected due to simplicity and inherent advantages [3]. The sizing parameterisation is done based on the geometric design shown in Fig. 1, from which b_{tx}=b_{pt}, and b_{rx}=b_{pr}, initially. The definition of the design parameters are conceived as follows:

$$\tau_s = \frac{\pi D_i}{N_s}, \tag{1}$$

$$b_{ps} = \tau_s - b_{sls}, \quad \text{[arc]} \tag{2}$$

$$b_{pt} = t_0 b_{pr}, \quad \text{[arc]} \tag{3}$$

$$\tau_r = \frac{\pi(D_i - 2g)}{N_r}, \tag{4}$$

$$b_{rx} = t_1 b_{pr}, \quad \text{[arc]} \tag{5}$$

$$b_{tx} = t_0 t_1 b_{pr}, \quad \text{[arc]} \tag{6}$$

where N_s and N_r are the number of stator and rotor slots respectively, while the rest can later be discerned in Table I. Based on initial sizing technique, the complete machine is drawn and solved using a 2D FEM suite developed in-house [16]. By setting the important design variables, the optimisation process is ready to be undertaken next.

III. Design Optimisation and Parametric Variation

Direct-drive wind generator systems are prone to size and mass enlargements, which impose a levy on the capital costs. Besides, with purely electrical excitation, additional copper losses are introduced by the DC windings imposes a limitation on the generator efficiency. For the proposed wind generator drive technology, the overall cost can be further increased through the power electronics if the generator kVA rating is too high. All of these important considerations are captured in a review paper in [17]. To this end, a simple multi-objective optimisation problem is applied as follows on the proposed DC-VRM wind generator:

$$\text{Minimise} \quad \begin{bmatrix} M_{Tot} \\ \frac{1}{\eta} \end{bmatrix}, \tag{7}$$

$$\textit{subject to} \quad \begin{matrix} 15\ \text{kW} \le P_{out} \le 20\ \text{kW} \\ PF > 0.8 \end{matrix}, \tag{8}$$

where M_A is the active mass, η is the efficiency, P_{out} is the generated output power and PF is the power factor. In total, nine (9) design variables are defined for the optimisation challenge, most of which are captured in Fig. 1(a) except for the DC field and AC phase current densities, J_{DC} and J_{AC}, respectively. Figs. 1(b) & 1(c) shows the constructed 12/10 DC-VRM generic design and flux density map in 2D FEM.

Though a major issue in DC-VRMs, the torque ripple has been deliberately left out of the optimisation procedure. From the design point of view, it presents a difficult exercise for the torque ripple to be addressed concurrently as either an objective or a constraint for the examined optimisation problem. This is because the torque ripple results from interactions between the DC and AC MMF harmonics and airgap permeance, with tendencies for exhibiting tradeoff with respect to the average torque. Moreover, the torque ripple is due to the presence of the cogging torque [2]. Hence, a new approach in this study seeks to address this problem by independently applying a simple rotor tooth-pairing technique on the selected optimum benchmark designs (OBDs), based on $b_{tx} < b_{pt}$ and $b_{rx} < b_{pr}$ according to Fig. 1.

While some techniques which vary split ratio, air gap length, ratio of AC to DC coil turns and stator/rotor tooth arc ratio have been applied to optimise torque ripple in DC-VRM [18], the rotor pairing scheme is yet to be attempted. In reference [19], it is shown that the rotor pairing scheme, among other techniques, when applied to PM-FSM yielded approximately a 13 % reduction in torque ripple without any reproach on the average torque.

Similarly, rotor pairing, as well as skewing, was applied in [20] in a partitioned stator WF-FSM, to reduce the on-load DC winding induced voltage which translates to torque ripple. By using the rotor pairing scheme, the results show that the peak-to-peak value of the on-load DC winding induced voltage in a 12/10-pole machine is reduced by 77 %, while the torque is reduced by 10 %. In the next section, the optimisation results are presented along with the torque ripple minimisation and performance evaluation of some selected OBDs.

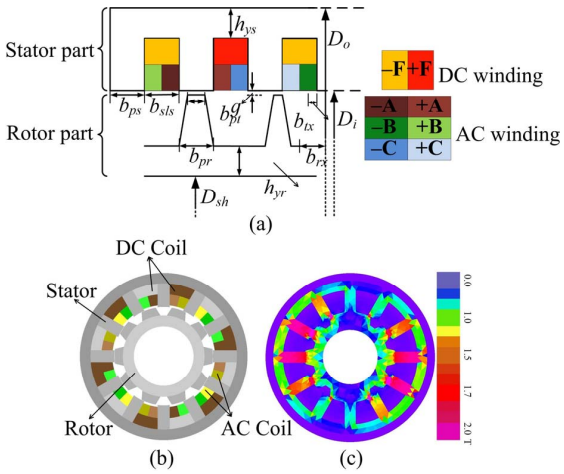

Fig. 1. DC-VRM basic design concepts: (a) geometric design and parameters, (b) 2D FEM drawing, and (c) flux density map in 2D FEM.

IV. Optimisation Results and Benchmark Performance Comparison

In this section, the DC-VRM optimisation results are presented and discussed, as well as the implementation of the proposed torque ripple reduction scheme in 2D and 3D FEM simulations. Based on the multi-objective optimisation problem, the generated optimal Pareto solutions are displayed as shown in Fig. 2, with three OBDs highlighted with reference to the observable tradeoffs in M_A and η across the optimal coastline.

The torque ripple reduction is undertaken on three selected OBDs based on the simple rotor tooth-pairing technique by varying adjacent rotor pole widths according to the ratios b_{tx}:b_{pt}, and b_{rx}:b_{pr} as illustrated in Fig. 1. While being emphasised for torque ripple reduction, the impact of the technique is also underscored for key performance data such as average torque (τ_e), power factor and efficiency as indicated in Fig. 3. During the design optimisation process, the rotor tooth-pairing ratios are kept as 1. It is clear that torque ripple ($\Delta\tau_e$) is not seriously impacted if ignored in the global optimisation, with the highest recorded value just slightly above 20 % among the three selected OBDs.

However, based on the rotor tooth-pairing ratios, one can see that a minimum value for $\Delta\tau_e$ is obtained in all three cases at 0.8. As a matter of emphasis, these reductions are more than half of their original values (52.5 % for OBD-I, 62.8 % for OBD-II and 59.7 % for OBD-III). It can be equally observed that at 0.8, a reasonable performance tradeoff for τ_e, η and PF is obtained in all three selected machines. For example, τ_e is only reduced approximately by 2 % and η by 1 %, while PF is unchanged.

To this end, highlights of the design variables and performance characteristics of the selected OBDs in 2D FEM are presented in Tables I and II, respectively. In Table II, OBD-II is prioritised and compared with results from a commercial 3D FEM package, since it provides the best tradeoff between M_A and η, as well as a modest proof of the design process. Consequently, certain performance resemblance can be seen from the 2D and 3D FEM solutions, with exception of the torque ripple and rated output power. As shown in Fig. 4, the latter may be due to some uncaptured end-effects and leakages, while meshing discrepancies could have resulted in the former as indicated in Fig. 5. Additional insights can be garnered by merely observing the meshing between 2D and 3D, and the corresponding effect on the cogging torque ($\Delta\tau_{NL}$) comparison in Table II. It confirms the culpability of the cogging torque for the torque ripple [2]. With finer meshing on the airgap surface of the stator and rotor 3D FEM models, the torque ripple evaluation should tally better but at the expense of increased computation time.

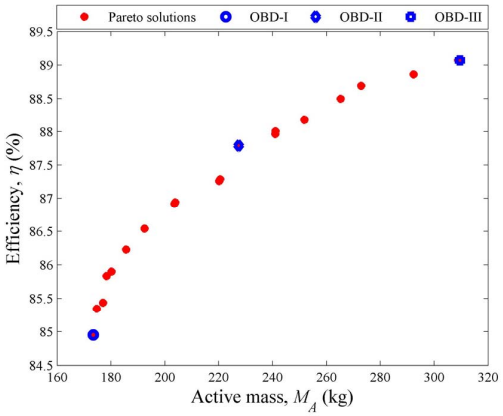

Fig. 2. Exhibition of the optimum trending designs and some selected benchmarks.

Further comparison of OBD-II is made with respect to a 15 kW direct-drive NO-PMSG wind generator as culled from [15]. It should be noted that P_{out} of some of the selected optimum machines (e.g., OBD-I and OBD-II) in 2D FEM as shown in Table II are slightly below the 15 kW benchmark due to tradeoffs in τ_e and $\Delta\tau_e$. It is important to note that, the kNm/m^3 values for the DC-VRM are typical for copper-excited electrical machines, compared to that of the NO-PMSG which is relatively high. In [10] and [20], it is estimated as 4.52 kNm/m^3 for the 22 kW DC-FRM and 66.5 kNm/m^3 for the 114.5 kW partitioned stator WF-FSM, respectively, although it has to be said that a current density of 26.8 A/mm^2 is used in the latter. To this end, 17.39 kNm/m^3 appears as a

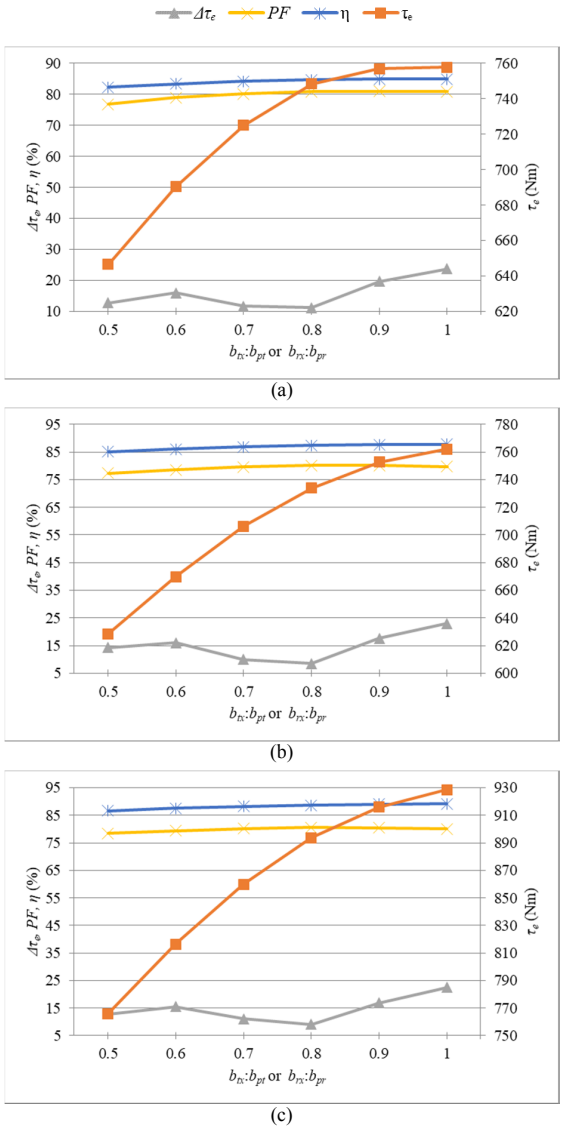

Fig. 3. Rotor tooth-pairing implemented for different optimum DC-VRM benchmarks: (a) OBD-I, (b) OBD-II, and (c) OBD-III (PF is given as percentage).

reasonable value for the 15 kW DC-VRM wind generator. In general, comparing OBD-II at par with the NO-PMSG as shown in Table II, it becomes clear that the main limitations of the proposed direct-drive DC-VRM are in terms of torque density and efficiency, no thanks to the absence of PMs.

The voltage regulation factor, which is determined as given in (9), is evaluated as shown in Table II:

$$\Delta U = \frac{U_S - U_0}{U_S} \times 100\%, \quad (9)$$

where U_0 and U_S are the generator's back-EMF and terminal voltage, respectively. It is seen that ΔU ranges from 8–18.3 % for the DC-VRM, which is a good indication of the generator's overload capability. Meanwhile, typical values of small-scale multi-phase PM wind generators are given in the range 15–40 % [11], [12].

In terms of efficiency, the evaluated values are within the expected range for the proposed DC-VRM wind generator concept. In Table III, a modest comparison is made with some related machine topologies from the literature [10]-[12], [15], [17], [20]. No doubt, it is clear that the obtained efficiency is very much satisfactory for a non-PM machine.

However, a much lower torque ripple and satisfactory behaviour of some critical performance constraints have been noted. The main argument for the proposed DC-VRM wind generators is that it provides a basis for harnessing an alternative and cheaper wind technology compared to PM generator variants. At the moment, OBD-II is benchmarked for fabrication and experimental validation based on the proposed 15 kW DC-VRM wind generator concept. However, due to the outbreak of the COVID-19 pandemic, the process is still ongoing. Meanwhile, a 3D outline of the finalised generator design, as well as the cut lamination of the stator and rotor core assemblage, are shown in Figs. 6 and 7, respectively.

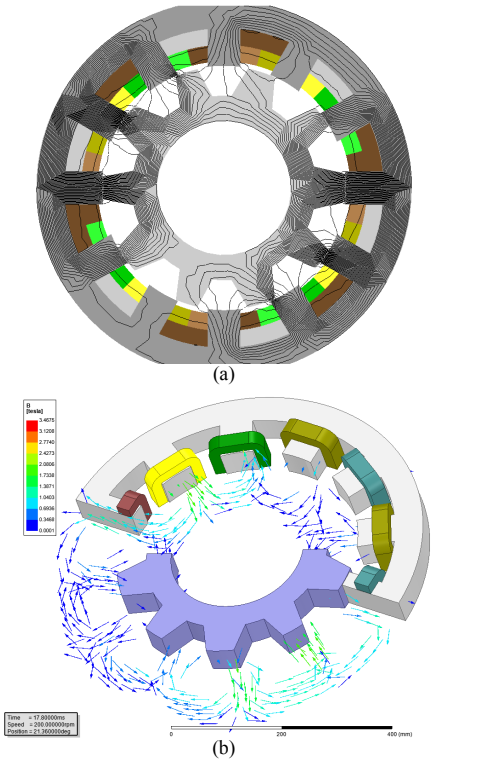

Fig. 4. Flux distribution lines in OBD-II: (a) 2D FEM full model (SEMFEM), and (b) 3D FEM quarter model (ANSYS Maxwell©.

TABLE I. OPTIMUM DESIGN PARAMETERS

	Parameters	OBD-I	OBD-II	OBD-III
D_o	Stator outer diameter (mm)	700	700	700
l_{st}	Stack length (mm)	86.5	109.6	148.1
D_i	Stator inner diameter (mm)	454.9	454.9	454.9
D_{sh}	Shaft diameter (mm)	250	250	250
b_{pr}	Rotor pole width (mm) [arc]	80.5	80.5	80.5
b_{sls}	Slot opening width (mm)	57.5	57.5	59.3
h_{ys}	Stator yoke height (mm)	35.3	52.4	58.1
h_{yr}	Rotor yoke height (mm)	45.0	47.1	47.0
t_0	Tapering index on rotor teeth	0.65	0.66	0.66
J_{DC}	DC current density (A/mm^2)	4.31	4.09	4.09
J_{AC}	AC current density (A/mm^2)	3.50	3.50	3.51
t_1	Rotor tooth-pairing ratio	0.8	0.8	0.8
g	Airgap thickness (mm)	0.8	0.8	0.8

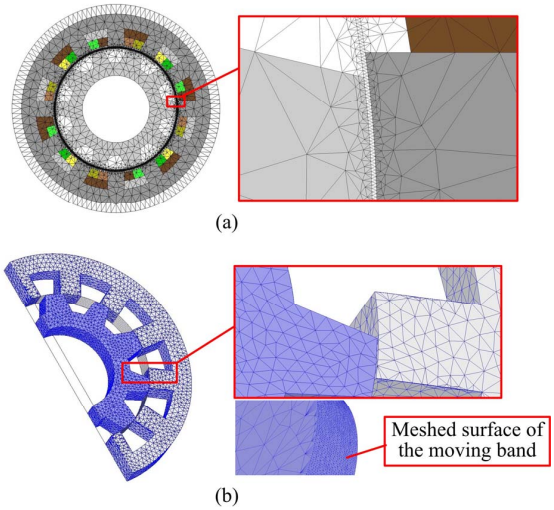

Fig. 5. Mesh architecture in: (a) 2D FEM, and (b) 3D FEM.

TABLE II. COMPARING THE OPTIMUM PERFORAMCNE

	[a]$\Delta\tau_{NL}$ %	$\Delta\tau_L$ %	[b]P_{Cu} kW	P_{core} W	PF -	η %	ΔU %	τ_e Nm	[c]M_{Cu} kg	[d]M_{Fe} kg	[e]M_{Tot} kg	τ_e/V_{act} kNm/m^3	P_{loss}/V_{act} kW/m^3	P_g kW
2D FEA: OBD-I	4.8	11.2	2.6	104.5	0.8	84.7	11.7	748.4	30.3	140.6	170.9	22.48	80.22	14.8
2D FEA: OBD-II	**7.4**	**8.5**	**1.9**	**120.2**	**0.8**	**87.4**	**9.7**	**732.0**	**28.5**	**195.9**	**224.4**	**17.39**	**50.16**	**14.6**
2D FEA: OBD-III	6.2	9.1	2.1	148.3	0.8	88.7	8.0	893.5	35.1	270.3	305.4	15.67	40.03	17.9
3D FEA: OBD-II	**20.5**	**24.6**	**1.9**	**92.2**	**0.7**	**87.4**	**18.3**	**651.3**	-	-	-	-	-	**14.1**
NOW-PMSG [15]	2.2	2.8	0.6	240	0.9	94.0	-	1000	18.9	58.2	84.86	72.22	250.7	15

[a]Cogging torque ($\Delta\tau_{NL}$); [b]copper loss (P_{Cu}); [c]mass of copper windings (M_{Cu}); [d]mass of steel (M_{Fe}); [e]total active mass (M_{Tot})

TABLE III. EFFICIENCY PERFORAMCNE COMPARISON OF DIFFERENT WIND GENERATORS

Reference	Rating	m^a	η	n
DC-VRM	14.6 kW	3	87.4 %	200 r/min
WF-FSM [9]	10 kW	3	78 %	360 r/min
DC-FRM [10]	22 kW	4	83.5 %	1500 r/min
PM-FSM [11]	9.8 kW	9	89 %	500 r/min
PM-FSM [12]	10.3 kW	12	87.8 %	500 r/min
NO-PMSG [15]	15 kW	3	94 %	150 r/min
Ferrite PM-FSM [17]	5 kW	3	77 %	30 r/min
PS WF-FSM [20]	114.5 kW	3	87.8 %	2795 r/min
Ferrite SPM[b] [20]	65.6 kW	3	90.6 %	2795 r/min
WRSM[c] [20]	216.7 kW	3	77.4 %	2795 r/min

[a]Phase number (m), [b]Surface PM machine (SPM), [c]Wound-rotor synchronous machine (WRSM)

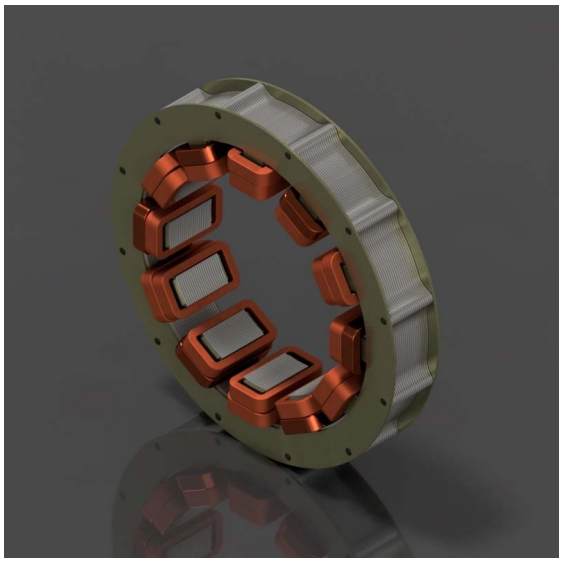

Fig. 6. 3D renditiion of the 15 kW DC-VRM prototype – OBD-II.

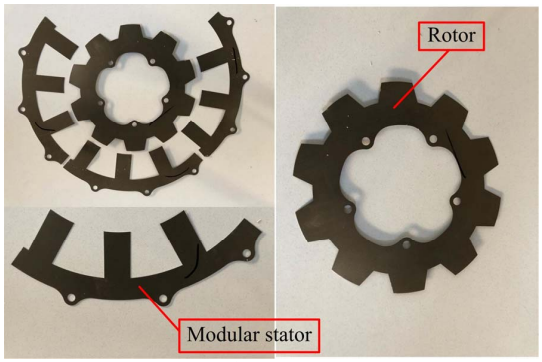

Fig. 7. Laser cut manufactured M400-50A electrical steel laminations of the proposed DC-VRM wind generator prototype – OBD-II.

V. CONCLUSION

In the study, a 15 kW DC-VRM design is proposed for direct-drive wind generator drives based on FEM and global optimisation. It is shown that the torque ripple constraint can be exonerated from the global optimisation framework, and later curtailed in the resulting optimum design candidates by using a simple rotor pole-pairing technique. At 0.8 pole-pairing ratio, more than 50 % reduction in torque ripple for the proposed DC-VRM is obtained, with negligible impact on the torque density. It should be mentioned that the findings are for a small-scale generator at a 15 kW power level, hence not large generators since it is well known that performance of copper-excited machines with respect to PM machines improves very much with power level. Hence, the much reduced performance figures compared to the PM design is expected. Typical torque density (17.4 kNm/m^3) and efficiency (87.4 %) of small-scale copper-excited electrical machines at 0.8 *PF* have been obtained for the optimum DC-VRM designs – this is good considering the advantages of brushless excitation and passive rotor.

ACKNOWLEDGMENT

This work is financially supported by the Department of Science and Innovation (DSI) in South Africa.

REFERENCES

[1] X. Liu and Z.Q. Zhu, "Electromagnetic performance of novel variable flux reluctance machines with DC-Field coil in stator," *IEEE Trans.Magn.,* vol.49, no.6, pp. 3020-3028, Jun. 2013.

[2] M. Lin, R. Qu, J. Li, and S. Jia, "Torque ripple reduction techniques for stator dc winding excited vernier reluctance machines," in *Proc. IEEEEnergy Convers. Congr. Expo.*, pp. 1–8, 2016.

[3] X. Liu and Z.Q. Zhu, "Stator/rotor pole combinations and winding configurations of varible flux reluctance machines," *IEEE Trans. Ind. Appl.*, vol. 50, no.6, pp. 3675-3684, Nov./Dec. 2014.

[4] D. Li, R. Qu and J. Li, "Topologies and analysis of flux-modulation machines," *IEEE Energy Conversion Congress and Exposition (ECCE)*, Montreal, QC, pp. 2153-2160, 2015.

[5] REN21, *Renewables 2020 global status report* (Paris: REN21 Secretariat), 2020. Available: www.ren21.net/gsr.

[6] U. Hoffmann, P. Bouwer and M. J. Kamper, "Direct grid connection of a slip-permanent magnet wind turbine generator," *IEEE Energy Conversion Congress and Exposition (ECCE)*, Phoenix, AZ, pp. 2373-2380, 2011.

[7] O. Keysan, "Future electrical generator technologies for offshore wind turbines," Eng. Technol. Ref., pp. 1-11, 2015.

[8] L. Szabó, "A Survey on Modular Variable Reluctance Generators for Small Wind Turbines," *IEEE Transactions on Industry Applications*, vol. 55, no. 3, pp. 2548-2557, May-June 2019.

[9] U. B. Akuru and M. J. Kamper, "Novel Experimentation of a 10 kW Geared Medium-Speed Wound-Field Flux Switching Wind Generator Drive," *IEEE Energy Conversion Congress and Exposition (ECCE)*, Portland, OR, 2018, pp. 6492-6498.

[10] C. H. T. Lee, K. T. Chau and C. Liu, "Design and Analysis of a Cost-Effective Magnetless Multiphase Flux-Reversal DC-Field Machine for Wind Power Generation," *IEEE Transactions on Energy Conversion*, vol. 30, no. 4, pp. 1565-1573, Dec. 2015.

[11] L. Shao *et al.*, "A comparative study on nine- and twelve-phase fluxswitching permanent-magnet wind generators," *IEEE Transactions on Industry Applications*, vol. 55, no. 4, pp. 3607-3616, Jul-Aug 2019.

[12] L. Shao, W. Hua, J. Soulard, Z. Q. Zhu, Z. Wu and M. Cheng, "Electromagnetic performance comparison between 12-phase switched flux and surface-mounted PM machines for direct-drive wind power generation," *IEEE Transactions on Industry Applications*, vol. 56, no. 2, pp. 1408-1422, Mar-Apr 2020.

[13] C. C. Pavel *et* al, "Substitution strategies for reducing the use of rare earths in wind turbines," *Resources Policy*, vol. 52, pp. 349-357, 2017.

[14] S. Jia, R. Qu, J. Li and D. Li, "Principles of Stator DC Winding Excited Vernier Reluctance Machines," *IEEE Transactions on Energy Conversion*, vol. 31, no. 3, pp. 935-946, Sept. 2016.

[15] J. H. J. Potgieter and M. J. Kamper, "Double PM-Rotor, Toothed, Toroidal-Winding Wind Generator: A Comparison With Conventional Winding Direct-Drive PM Wind Generators Over a Wide Power Range," *IEEE Transactions on Industry Applications*, vol. 52, no. 4, pp. 2881-2891, Jul-Aug. 2016.

[16] SEMFEM: www0.sun.ac.za/semfem/index.html

[17] I. Boldea, L. Tutelea and F. Blaabjerg, "High power wind generator designs with less or no PMs: An overview," *17th Int'l Conference on Electrical Machines and Systems (ICEMS)*, Hangzhou, 2014, pp. 1-14.

[18] S. Jia, R. Qu and J. Li, "Design considerations and parameter optimization of stator wound field synchronous machines based on magnetic the gear effect," *IEEE Energy Conversion Congress and Exposition (ECCE)*, Montreal, QC, 2015, pp. 5195-5202, 2015.

[19] W. Xu, J. Zhu, Y. Zhang, and J. Hu, "Cogging torque reduction for radially laminated flux-switching permanent magnet machine with 12/14 poles," *IECON 2011 - 37th Annual Conference of the IEEE Industrial Electronics Society,* Melbourne, VIC, pp. 3590-3595, 2011.

[20] Z. Wu, Z. Zhu, C. Wang, J. Mipo, S. Personnaz and P. Farah, "Analysis and Reduction of On-Load DC Winding Induced Voltage in Wound Field Switched Flux Machines," *IEEE Transactions on Industrial Electronics*, vol. 67, no. 4, pp. 2655-2666, April 2020